minerals

MDPI

Article

Applying Data-Driven-Based Logistic Function and Prediction-Area Plot to Map Mineral Prospectivity in the Qinling Orogenic Belt, Central China

Hongyang Bai [1,2], Yuan Cao [3], Heng Zhang [3], Wenfeng Wang [1,2,4,*], Chaojun Jiang [3] and Yongguo Yang [1,2]

1 School of Resources and Geosciences, China University of Mining and Technology, Xuzhou 221116, China
2 Key Laboratory of Coalbed Methane Resources and Reservoir Formation Process of the Ministry of Education, China University of Mining and Technology, Xuzhou 221000, China
3 The Second Geology Prospecting Institute of Henan Bureau of Geology and Mineral Exploration and Development, Zhengzhou 451464, China
4 School of Geology and Mining Engineering, Xinjiang University, Urumqi 830047, China
* Correspondence: wangwenfeng@cumt.edu.cn

Abstract: This study combines data-driven-based logistic functions with prediction–area (P–A) plot for delineating target areas of orogenic Au deposits in the eastern margin of the Qinling metallogenic belt, central China. First, appropriate geological and geochemical factors were identified, optimized, and transformed into a series of fuzzy numbers with a range of 0–1 through a data-driven-based logistic function in order to determine the evidence layer for prospecting orogenic Au. In addition, the P–A plot was derived on the above evidence layers and their corresponding fuzzy overlay layers to pick out a proper prediction scheme, in the process of which acidic magmatic activity proved to be the most important factor of ore-controlling. Moreover, to further prove the advantages of this method, a traditional linear knowledge-driven approach was carried out for comparative purposes. Finally, based on concentration–area (C–A) fractal theory, the fractal thresholds were determined and a mineral prospecting map was generated. The obtained prediction map consisted of high, medium, low, and weak metallogenic potential areas, accounting for 2.5%, 16.1%, 38.4%, and 43% of the study area, containing 2, 3, 1, and 0 of the 6 known mine occurrences contained, respectively. The P–A plot indicated that the result predicted 83% of Au deposits with 17% of the area, confirming the joint application of the data-driven-based logistic function and P–A plot to be a simple, effective, and low-cost method for mineral prospectivity mapping, that can be a guidance for further work in the study area.

Keywords: mineral prospectivity mapping; logistic function; prediction-area; concentration-area; orogenic Au

Citation: Bai, H.; Cao, Y.; Zhang, H.; Wang, W.; Jiang, C.; Yang, Y. Applying Data-Driven-Based Logistic Function and Prediction-Area Plot to Map Mineral Prospectivity in the Qinling Orogenic Belt, Central China. *Minerals* **2022**, *12*, 1287. https://doi.org/10.3390/min12101287

Academic Editor: Behnam Sadeghi

Received: 9 September 2022
Accepted: 11 October 2022
Published: 13 October 2022

1. Introduction

Mineral prospectivity mapping (MPM) is a comprehensive area of study, during which geological engineers identify metallogenic target areas with known information and data in the study area to guide further exploration. It is essentially a classification technique [1], by which the study area can be divided into areas with high, moderate, and low favorability of mineralization [2,3]. The process of MPM generally includes the understanding of the metallogenic model, the identification of ore-controlling factors, data treatment or transformation, and finally the integration of these results to describe the ore-forming target area [4]. Simply, its objective is to portray the smallest area usually containing the most mineral deposits. In the above process, however, two key difficulties remain. One is to convert evidence layers with different orders of magnitude values into the same space and integrate them [5]; the other is to determine a group of reasonable thresholds to demarcate the study area [2].

Recent decades have witnessed researches on the aforementioned issues by many scholars. For example, Behera et al. [6] applied C–A fractal and fuzzy analytic hierarchy processes to predict geochemical anomalies and mineral prospects in Sonakhan Greenstone Belt in central India. Yousefi et al. [1,7] compared the effectiveness of Boolean logic, a geometric mean model, and expected value model in metallogenic prediction. Carranza [8] employed data-driven evidence confidence functions to predict the mineralization of gold deposits in Baguio District, Philippines. Knox-Robinson [2] used vector fuzzy logic to integrate spatial data and study the metallogenic prospect of gold deposits in Kalgoorlie Terrane orogenic belt, Western Australia. Carranza [9] proposed a Wildcat model based on logic function.

All the methods described above generally fall into three categories [5,10,11]. The most common one is the knowledge-driven method that mainly assesses mineralization evidence based on the knowledge of geological experts and assigns different weights to each mineralization factor. It is generally suitable for study areas with low exploration levels [9], in which considerable mineralization data are absent. Among them, fuzzy sets and fuzzy logistics, proposed by Zadeh [12], have been widely applied and proven to be of great value in MPM by many geologists [2,11,13–20]. However, this method has the weakness of suffering from experts' bias, thus resulting in different experts often having different opinions [1]. Another approach is the traditional data-driven method that can better establish the relationship between known mines and various evidence layers for metallogenic prediction [21–26]. Nevertheless, its deficiency is that it requires a training batch of known mines to establish this connection, rendering it infeasible in areas with low exploration levels. As a result, it would be a deviation from the fact that unknown deposits have a lesser chance of being involved in such training. In addition, there are approaches (or systems) of integration [27] or hybridization of the two aforementioned methods [28–33]. However, most of these still cannot overcome the above dilemma or remain in development.

However, there are very few ways to overcome the bias of metallogenic prediction due to personal knowledge limitations or preferences. In order to solve the above defects, many geologists began to try empirical function for MPM [8,9,16,28,34]. In these methods, a data-driven approach based on logistic functions proposed by Yousefi et al. [7,35,36] and Yousefi and Carranza [1], in which weights can be assigned to the evidence layers without experts' bias and the known mines, is able to alleviate the aforementioned drawbacks. At the same time, with the development of computers, big data and artificial intelligence technology have been applied to MPM more and more frequently due to their advancement and economy. For example, Liu et al. [37] applied convolutional neural networks in prospecting predictions of the Zhaojikou Pb–Zn ore deposit in Anhui Province, China; Zuo and Xu [38] proved the advantages of graphical deep learning models compared with convolutional neural networks in metallogenic prediction; Zhou et al. [39] summarized the research progress of big data technology in Earth science and considered it to be an important technology for future breakthroughs in this field.

In this study, the MPM of orogenic Au was implemented by combining logistic function with P–A plot based on the analysis of regional geological background and ore-controlling factors, especially a considerable amount of stream sediment geochemical data. The prospectivity map shows the delineated middle–high favorable areas, accounting for 17% of the study area and encompassing five out of the six known mines, would be an ideal prediction output

2. Geological Setting

The study area lies in the southwest of Henan province, central China, covering an area of 1001 km^2. It is located tectonically at the junction between the southern margin of the North China Plate and the northern margin of the Yangtze Plate (the central and eastern part of the Qinling structural belt), with the Jingziguan–Shigang complex syncline generating the Xixia fault depression basin [40,41]. Crossing four metallogenic zones (north

Qinling orogenic belt, south Qinling fold belt, Xixia–Tongbai polymetallic metallogenic belt, and the Danjiangkou gold–silver–vanadium–antimony metallogenic zone), the study area is characterized by complex geological conditions, frequent magmatic activities, and significant structural deformation (regional) metamorphic effects. Consequently, the metallogenic geological conditions are superior, with vanadium and gold as the main metals and marbles and limestones as the main non-metallic minerals, resulting in an area with rich reserves and prospecting potential [41].

The Au deposits in the region are mainly the orogenic belt type, whose metallogenic geological conditions mainly include ore-bearing rocks, ore-controlling structures, and magma activities [41–45]. However, because the ore-bearing rocks could not be more complex and diverse, and a variety of rocks can generate ore-bearing rocks when other mineralization conditions are in place, only ore-controlling structures and magmatic activities are considered in this study, as per common engineering practice. Magma, as the main heat source, plays an important role in the formation of gold deposits. It can not only provide a corresponding motive force for element migration and aggregation, but also supply the matter source [46] (Craw et al., 2006). As Mao et al. [47] and Chen et al. [48] mentioned, most gold deposits are related to Mesozoic granites in the Xiaoqinling–Xiong'ershan region. At the same time, the tectonic belt plays a crucial role in controlling mineralization, and the known gold spots are mainly distributed along the fault zone from the northwest to southeast. The location and simple geological maps of the study area are shown in Figure 1.

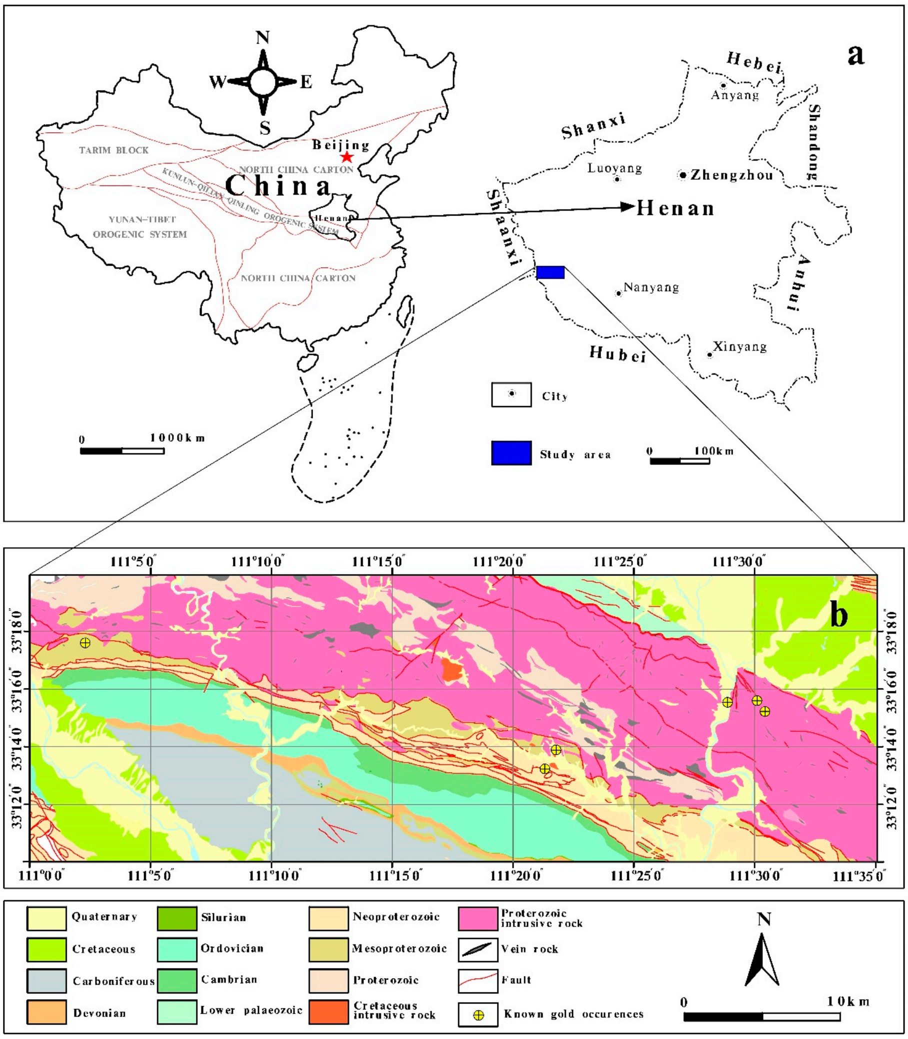

Figure 1. (**a**) Location of the study area, and (**b**) simple geological map of the study area (After [49]).

3. Data Set

3.1. Data Sources

In this study, we used the 1:50,000 regional geological map and 1:50,000 stream sediment survey data prepared by the Second Geology Prospecting Institute of Henan Bureau of Geology and Mineral Exploration and Development. In total, 4036 samples (Figure 2) were collected, processed and analyzed, with a sampling density of 4–6 points per square kilometer in about 1000 square kilometers in the study area. Each of the original samples weighed more than 150 g with a particle size of less than 60 mesh (<216 μm).

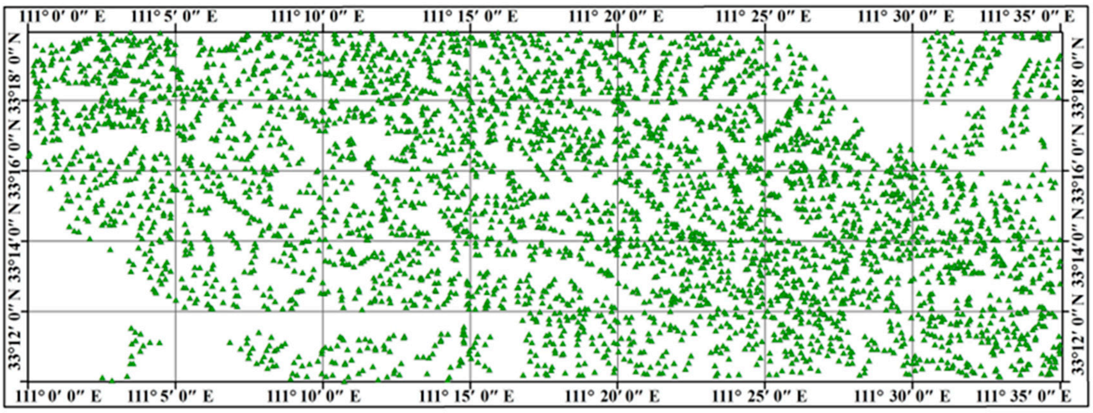

Figure 2. Location map of stream sediment samples (after [49]).

The concentrations of Au, Ag, As, Sb, Cu, Pb, Zn, Mo, W, and Cd were analyzed by using graphite furnace atomic absorption spectrometry (Au), atom emission spectrometry (Ag), atomic fluorescence spectrometry (As and Sb), and inductively coupled plasma optical emission spectrometry (Cu, Pb, Zn, Mo, W, and Cd). The detection limits were 0.3 ppb for Au, 0.02 ppm for Ag, 0.2 ppm for As, 0.04 ppm for Sb,1 ppm for Cu, 1 ppm for Pb, 5 ppm for Zn, 0.3 ppm for Mo, 0.3 ppm for W, and 0.04 ppm for Cd.

Tight quality control was maintained at every stage of the process, in accordance with [50,51].

3.2. Data Preprocessing

On the basis of [52], we determined a proper cell with 200 m × 200 m for all of the evidence maps. Subsequently, the geological data and geochemical data were processed to obtain evidence values in each cell. In this way, the study area contained a total of 25,024 cells.

On the basis of the 1:50,000 geology survey, the main geological information related to the mineralization, such as magmata and faults, was extracted as the evidence layers. Meanwhile, based on the measurement of the 1:50,000 stream sediment survey, stage factor analysis (SFA), as proposed by Yousefi et al. [7], was performed to assess the multiple elements closely related to gold mineralization in the study area. Subsequently, the corresponding multi-element factors were grid-processed to determine their value in each cell.

3.2.1. Geological Evidence, Main Heat Sources, and Faults

In this study, the granite vein and the Yanshanian granite porphyry were extracted as the evidence layers and the distance from the intrusion contact was used as the indicator criterion. However, the further from the intrusion, the less the possibility of mineralization; thus, the inverse square of the distance from intrusive was taken as the evidence value in each cell (Figure 3a). It is generally accepted that faults are important channels for the movement of geological fluids [53]. Without faults, there could be little migration and enrichment of elements; as a result, it would be impossible to generate gold deposits as well. Consequently, we took the proximity to fault as the evidence value, whose method of acquisition was similar to that of the heat source (Figure 3b).

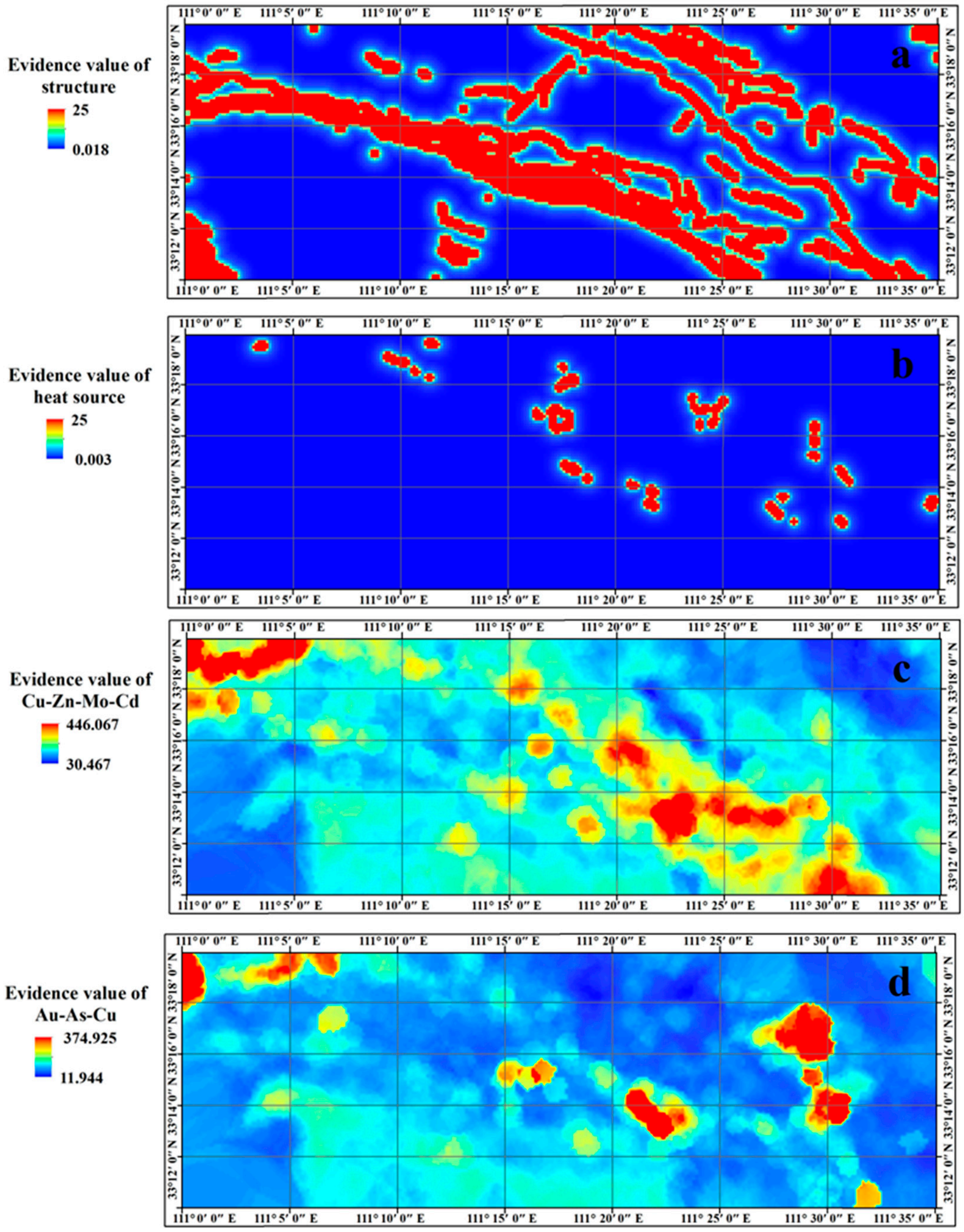

Figure 3. Evidence values of: (**a**) structure; (**b**) heat source; (**c**) Cu–Zn–Mo–Cr factor; and (**d**) Au–As–Pb factor.

3.2.2. Geochemical Evidence

Stage factor analysis, based on the principal component analysis developed by Yousefi et al. [7] as an optimized method, was performed on 4036 samples of 10 elements to obtain multi-element geochemical anomaly factors, using the statistical product and service solutions (SPSS) platform.

From the results of the staged factor analysis (Table 1), two indicator factors (Figure 3c,d) were obtained to reflect the presence of orogenic gold deposits: F1 (Cu–Zn–Mo–Cd) and F2 (Au–As–Pb). Elements with high factor loading values (greater than 0.6 with bold) in the third and fourth stages of the two factors could be used as indicator factors based on geochemical criteria to define exploration targets. In terms of F1 (Cu–Zn–Mo–Cd), these are obviously sulfurophile elements that often form chalcopyrite, sphalerite, molybdenite, and greenockite in nature, respectively. As we all know, S is usually considered to be the mineralizer of Au or an important component of Au-loaded minerals due to the extremely weak activity of Au; sometimes, the source of Au can be transformed into the source of S. In terms of F2 (Au–As–Pb), these are typical low-temperature elements with similar geochemical characteristics; thus, As and Pb are often found in the leading edges of gold belts. Generally, Au, As, and Pb have a strong migration ability in ore-forming fluids, and are most likely to migrate or accumulate along those secondary fracture or ductile shear zones.

Table 1. Rotated factor matrix of staged factor analysis and data of samples from the study area. Loadings in bold represent the selected elements based on a threshold of 0.6 (the absolute threshold value) for each stage.

First Main Phase						Second Main Phase			
First Stage			Second Stage			Third Stage		Fourth Stage	
Element	**F1**	**F2**	**Element**	**F1**	**F2**	**Element**	**F1**	**Element**	**F2**
Au	−0.1	**0.726**	Au	−0.07	**0.719**	Cu	**0.698**	Au	**0.681**
Ag	0.48	0.592	As	0.153	**0.803**	Zn	**0.797**	As	**0.819**
As	0.118	**0.785**	Cu	**0.719**	−0.029	Mo	**0.758**	Pb	**0.783**
Sb	0.184	0.304	Pb	0.291	**0.713**	Cd	**0.838**		
Cu	**0.723**	−0.002	Zn	0.72	0.384				
Pb	0.257	**0.685**	Mo	**0.771**	0.072				
Zn	**0.692**	0.354	Cd	**0.812**	0.16				
Mo	**0.761**	0.1							
W	0.266	0.235							
Cd	**0.803**	0.195							

4. Methodology

4.1. Logistic Function

Different evidence layers have values of diverse orders of magnitude; therefore, they are incomparable and cannot be superimposed to generate a prospecting map. In this context, logistic function was proposed by Bishop (2006) [54], with which discrete data of different orders of magnitude can be converted to continuous values of 0–1, thus avoiding arbitrary division of evidence value by traditional knowledge-based methods. In addition, Yousefi and Carranza [5] proposed an optimized method based on logic function, in which the parameters can be calculated in a data-driven way, so that the converted value can perfectly fall between 0–1.

Therefore, we used an S-shape logistic function to transform the evidence values to obtain fuzzy numbers with a range of 0–1, which could be definite proxies of the evidence values.

$$F_{EV} = \frac{1}{1 + e^{-s(EV-\mathrm{i})}} \tag{1}$$

The S–shaped logistic function, as shown in Equation (1) [5], where EV and F_{EV} are the evidence value and fuzzy score, respectively, while s and I are unknown parameters, has been used by a number of geologists as an efficient tool for MPM, most of whom have obtained anticipative results. However, as Yousefi and Nykänen [5] mentioned, the selection of the s and I parameters in logistic function is often subjective, because different experts often have different preferences. Moreover, some subjectively selected parameters cannot achieve continuous fuzzy numbers. Thus, such experience-based parameters sometimes yield different evidence values with similar or concentrated fuzzy numbers, resulting in the fuzzy score being a poor representative of the source data.

Therefore, Yousefi and Nykänen [5] suggested defining the maximum and minimum values of F_{EV} as close to 1(0.99) and close to 0(0.01), which represent the most and least important evidence value. With known values of EV_{max} and EV_{min} (the maximum and minimum values of EV) as well as F_{Evmax} and F_{Evmin} (the maximum and minimum values of F_{EV}, respectively), Equations (2) and (3) can easily be solved to find s and i. In this way, a data-driven fuzzy score is obtained, which avoids the distortion of conversion caused by experts' subjective bias.

$$\begin{cases} F_{Evmax} = \frac{1}{1+e^{-s(EV_{max}-i)}} \\ F_{Evmin} = \frac{1}{1+e^{-s(EV_{min}-i)}} \end{cases} \tag{2}$$

$$\begin{cases} s = \frac{9.2}{EV_{max}-EV_{min}} \\ i = \frac{EV_{max}+EV_{min}}{2} \end{cases} \tag{3}$$

4.2. Prediction-Area Plot

The P–A plot, a method proposed by Yousefi and Carranza [55], can not only assign weight to each evidence layer, but also evaluate its prediction ability, so as to select a more appropriate evidence layer for MPM. Specifically, it consists of two curves, one corresponding to the left axis, which represents the proportion of the number of mines predicted by the evidence layer to the total, and the other corresponding to the right axis, which represents the proportion of the area account for the total area. There is an intersection point between the two curves, and the higher the intersection point is, the stronger the predictive ability of the evidence layer is. In other words, the higher the intersections of the evidence layer on the P–A plot, the stronger the intrinsic association with the mineral deposit.

5. Results

5.1. Data Transformation

For orogenic gold deposits, faults usually play a role as an activity space or even a storage space for ore-containing hydrotherms [45,56,57]. It is generally believed that the further from the fault, the lower the degree of profitability of the mineralization; thus, the inverse square of the proximity to the fault can be applied as the evidence value. When the evidence value is 0 (i.e., the cell contains the fault itself), its inverse square does not exist; therefore, we manually assign it the maximum value. Based on the GIS platform, the proximity to fault of each cell is computed, the maximum and minimum of whose inverse square are calculated to be 25 and 0.018, respectively. Using Equations (2) and (3), the corresponding s and i values were acquired as 0.3683 and 12.5090. Proximity to the intrusion was used as the data set for the heat source. The further from the intrusive contact, the lower the degree of profitability of mineralization; therefore, we applied the inverse square as the evidence value as well. Due to the nonuniformity of sampling points, the ordinary kriging interpolation [58,59] was conducted on the two multi-element factors (Cu–Zn–Mo–Cd factor and Au–As–Pb factor) to obtain the evidence value of each cell, verifying that they conformed to the normal distribution.

After obtaining the evidence values of the above layers, Equation (1) was utilized to obtain the fuzzy score in each cell (the maximum value was 0.99, and the minimum value was 0.01), which represented the favorable degree of mineralization. The parameters used in the conversion process are shown in Table 2 and the obtained fuzzy score layers are depicted in Figure 4.

Table 2. Parameter values calculated for each evidence layer.

Evidential Layer	s	i
Structure	0.3683	12.5090
Heat source	0.3680	12.5015
Cu-Zn-Mo-Cd-	0.0221	238.2672
Au-As-Pb	0.0253	193.4347

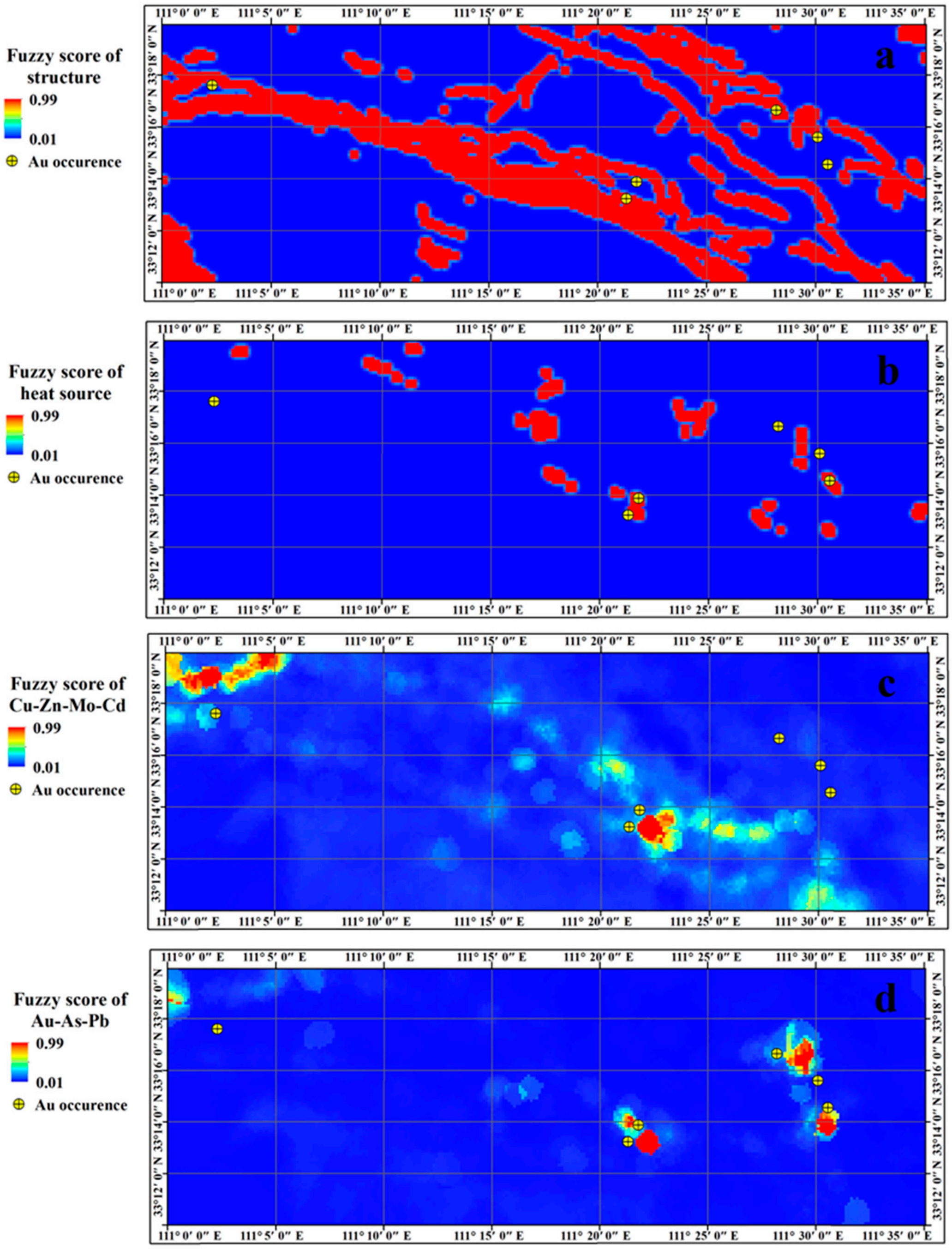

Figure 4. Fuzzy score of: (**a**) structure; (**b**) heat source; (**c**) Cu–Zn–Mo–Cd factor; and (**d**) Au–As–Pb factor.

In order to confirm whether the fuzzy score could be a good representation of the mineralization favorability, the obtained fuzzy score layers (Figure 4a–d) were compared with the evidence value layers (Figure 3a–d) for a comparable purpose. The comparison revealed that both of them were highly similar and the former exhibited a slight convergence compared with the latter, although only in areas where the evidence values had an unobvious anomaly; therefore, it proved better to identify the real anomalies.

This is consistent with the research of Bishop [58] and Yousefi et al. [7] that non-linear transformations (such as the logistic function) yield an optimal decision boundary between different classes of a variable for classification, thus boosting stronger discrimination between anomaly and background values. Therefore, we believe that the data-driven logistic function used in this study is appropriate due to its ability of transforming evidence values of different magnitudes to fuzzy scores with a 0–1 range and retaining the relative importance.

5.2. Evaluation of Fuzzy Evidence Layers

Before conducting the fuzzy overlay, we performed a P–A plot, which could evaluate the mineralization advantage of each layer objectively, to quantify its prediction ability. This method employs the ratio of predicted gold deposits to total deposits, versus the ratio of the accumulated area to total area as indicators based on the known gold deposits [10].

The P–A plot of the evidence layer is shown in Figure 5. The intersection of the two curves represents the prediction ability of the evidence layer. The higher the intersection, the stronger the prediction ability, and the closer it is to mineralization.

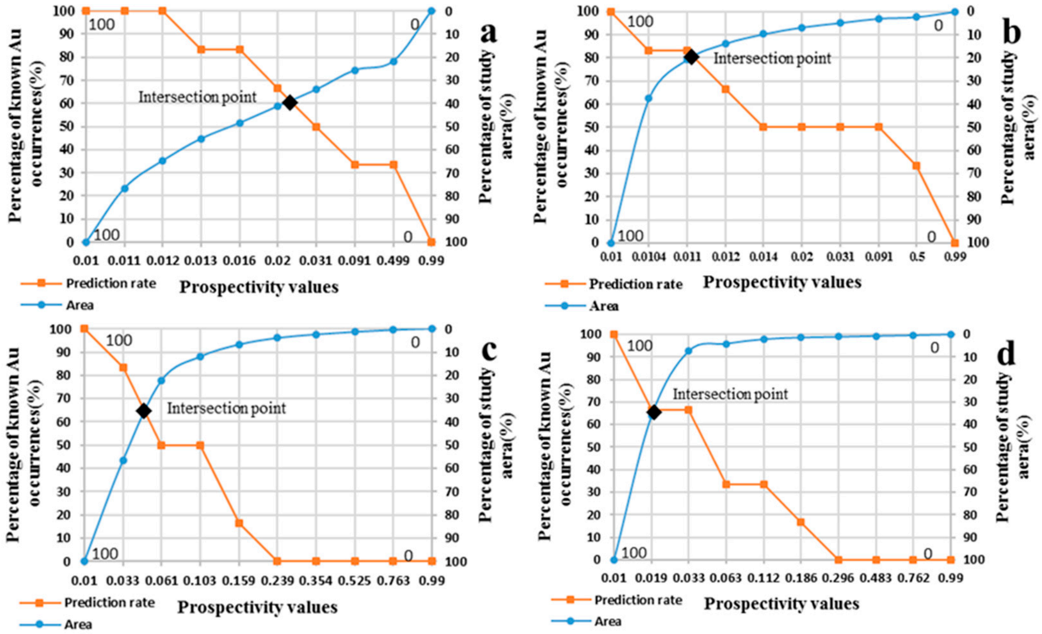

Figure 5. Prediction area (P–A) plot of each layer: (**a**) structure; (**b**) heat source; (**c**) Cu–Zn–Mo–Cr factor; and (**d**) Au–As–Pb factor.

5.3. Integration

As can be seen from Table 3, the prediction capability of each fuzzy evidence layer was quite different. The best one was the heat source, with a value of 81, which significantly exceeded other layers. In order to better determine the relationship between each fuzzy evidence layer and mineralization, we conducted fuzzy overlay with a γ value of 0.95 [60] to integrate these layers.

Table 3. Prediction ability of each evidence layer.

Evidential Layer	% of Known Au Occurrences	% of Study Area
Figure 4a (structure)	61	39
Figure 4b (heat source)	81	19
Figure 4c (Cu–Zn–Mo–Cr)	65	35
Figure 4d (Au–As–Pb)	67	33

The fuzzy evidence layers with prediction ability greater than or equal to 81, 67, 65, and 61 were integrated separately to obtain three overlay maps (Figure 6) that were then estimated by P–A plot, and their evaluation results are shown in Table 4.

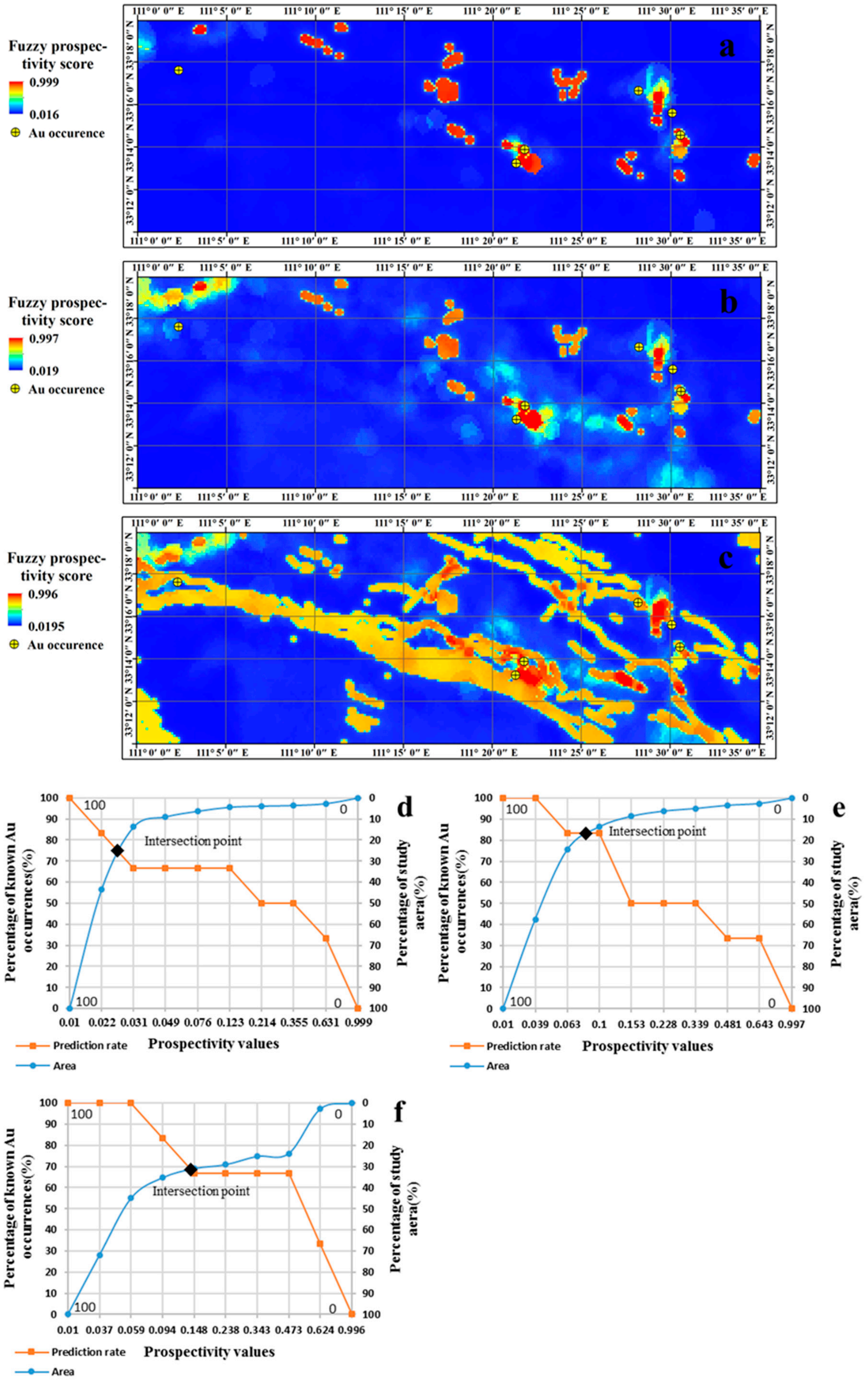

Figure 6. Perspectivity scores: (**a**) integrated with Figure 4b,d; (**b**) integrated with Figure 4b–c; and (**c**) integrated with Figures 4b–d and 3a; (**d**) P–A plots of Figure 6a; (**e**) P–A plots of Figure 6b; (**f**) P–A plots of Figure 6c.

Table 4. Prediction ability of each integrated layer.

Fuzzy Prospectivity Map	% of Known Au Occurrences	% of Study Area
Figure 6a	75	25
Figure 6b	83	17
Figure 6c	68	32

Although there are many similarities between Figure 6a,b, the latter has a slightly stronger predictive value (Figure 6d,e, and Table 4). However, we also noticed that the corresponding forecasting capacity from Figure 6d to 6f possessed a trend of increasing first and then declining. Among them, Figure 6e reached a maximum with a prediction rate of 84%; at this point, the evidence layers for integration were Figure 4b–d, with prediction rates of 81%, 65%, and 67%, respectively. This phenomenon is strange, because several layers with lower prediction ability have a better result when integrated. In spite of this, it is in line with a previous study [55]. What is interesting is that the prediction rate of Figure 6c dropped significantly when faults were added for integration. This may be caused by the multi-phase superposition of tectonic movements in this area, leading to the development of a large number of faults, whereas there is no magmatic hydrothermal activity in some faults.

In summary, it has been proven that the heat sources, Cu–Zn–Mo–Cd factor, and Au–As–Pb factor are the most important aspects in the mineralization process. Consequently, Figure 6b could be used as the ideal perspectivity map in the study area.

5.4. Fuzzy Prospectivity Score Obtained Linearly (A Comparison)

Carranza (2008) [22] suggested that two or more methods should be conducted in MPM to determine a proper metallogenic target area. Thus, in order to further demonstrate the superiority of logistic functions, we employed the knowledge-driven method to divide the evidence layers on the four evidence layers of Figure 3 into 10 classes at specific intervals, and assigned a mineralization favorability weight to each class linearly based on expert judgment for comparison purposes (Figure 7).

Subsequently, fuzzy gamma (γ = 0.95) operation was performed, and the fuzzy prospectivity score and matching P–A plot were obtained (Figure 8a,b). According to Figure 8b, the intersection value was 77, obviously lower than that of Figure 6b (83). The above results indicate that that weighting the evidence layer using the logistic function not only avoids subjective judgment, but also yields a higher prediction rate compared with the traditional discrete linear method. This is consistent with the findings of Yousefi and Carranza [1].

5.5. To Determine the Thresholds

As Mandelbrot [61–63] and Carlson [64] mentioned, in many cases, ore deposits are characterized by aggregation and fractal distribution. Therefore, in order to determine the high, moderate, low and weak areas of the mineralization more accurately, we employed the C–A method to de-fuzzify Figure 6b and obtain a prospectivity map. This method was proposed by Cheng [65], and has been used and approved by a number of geologists [66–72]. It applies the logarithm of the concentration and the logarithm of the corresponding area greater or equal to concentration as the X-axis and Y-axis, respectively, which can reflect the fractal characteristics inherent in the prediction map. According to this method, in the log-log graph, the consistent slope represents a fractal dimension, and the concentration value corresponding to the fractal point could be used as the threshold for differentiating the favorable, unfavorable, and intermediate areas of mineralization [5].

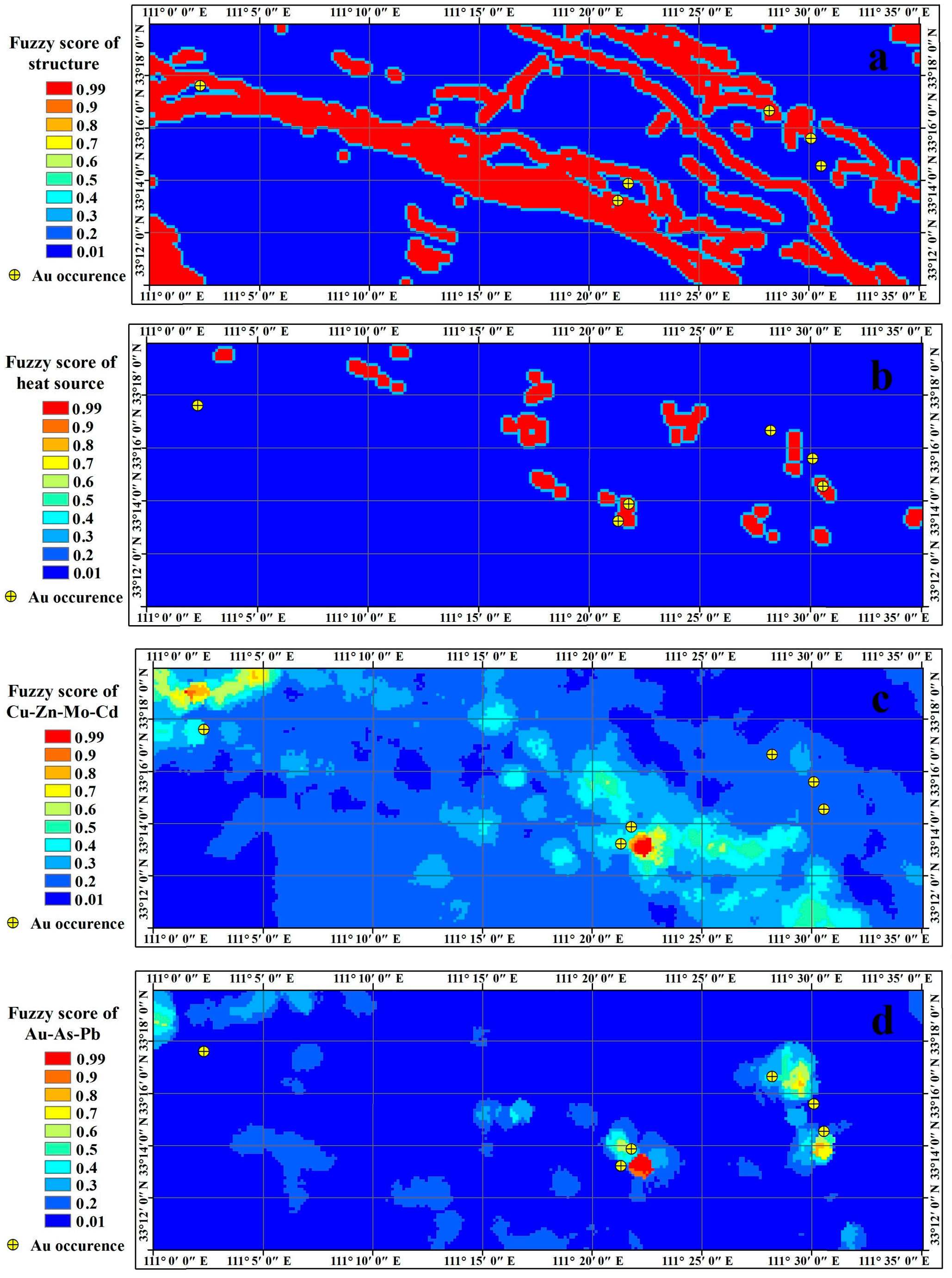

Figure 7. Fuzzy score obtained using the knowledge-driven approach: (**a**) structure; (**b**) heat source; (**c**) Cu–Zn–Mo–Cr factor; and (**d**) Au–As–Pb factor.

In this study, the logarithm of the fuzzy score and the logarithm of the cumulative area were taken as the X-axis and Y-axis, respectively (Figure 9a). Three inflection points were obtained (−1.41, −1.11, and −0.19) and the corresponding fuzzy prediction values (0.039, 0.078, and 0.643) were acquired, which then were used to divide the study area into four parts (Figure 9b). The resulting high-potential area accounting for 2.5% of the study area, containing two known Au occurrences, the moderate-potential area accounting for 16.1% of the study area with three, the low potential area accounting for 38.4% of the study area with one Au occurrence, and the very low-potential area accounting for 43% of the study area with no Au occurrences, would be an ideal metallogenic prediction map.

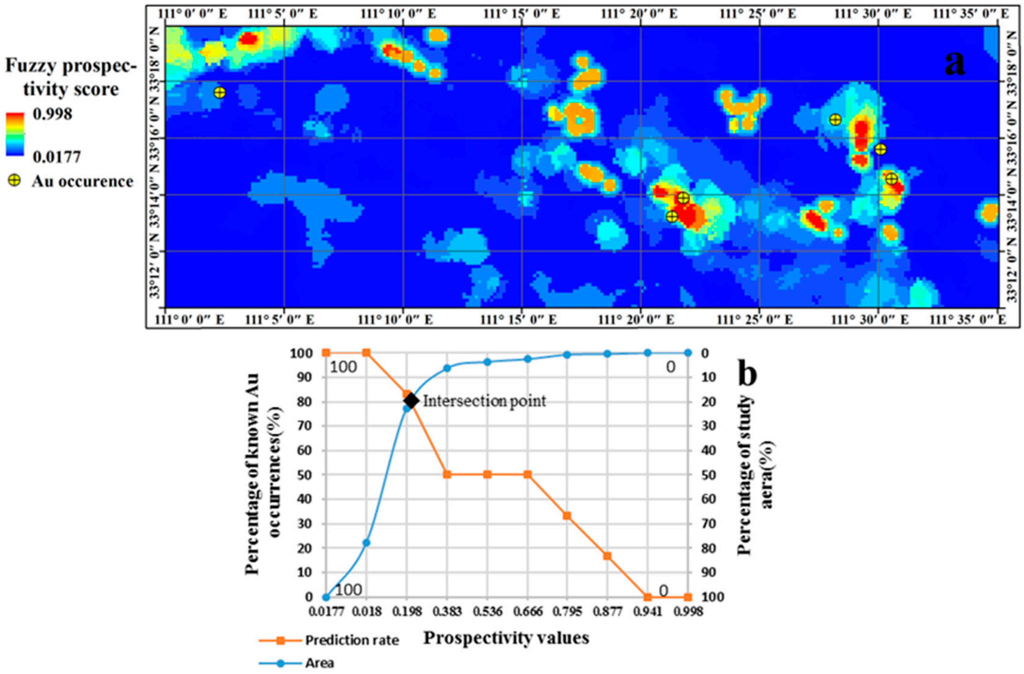

Figure 8. (**a**) Fuzzy prospectivity score integrating by Figure 6–d; (**b**) P–A plot of Figure 8a.

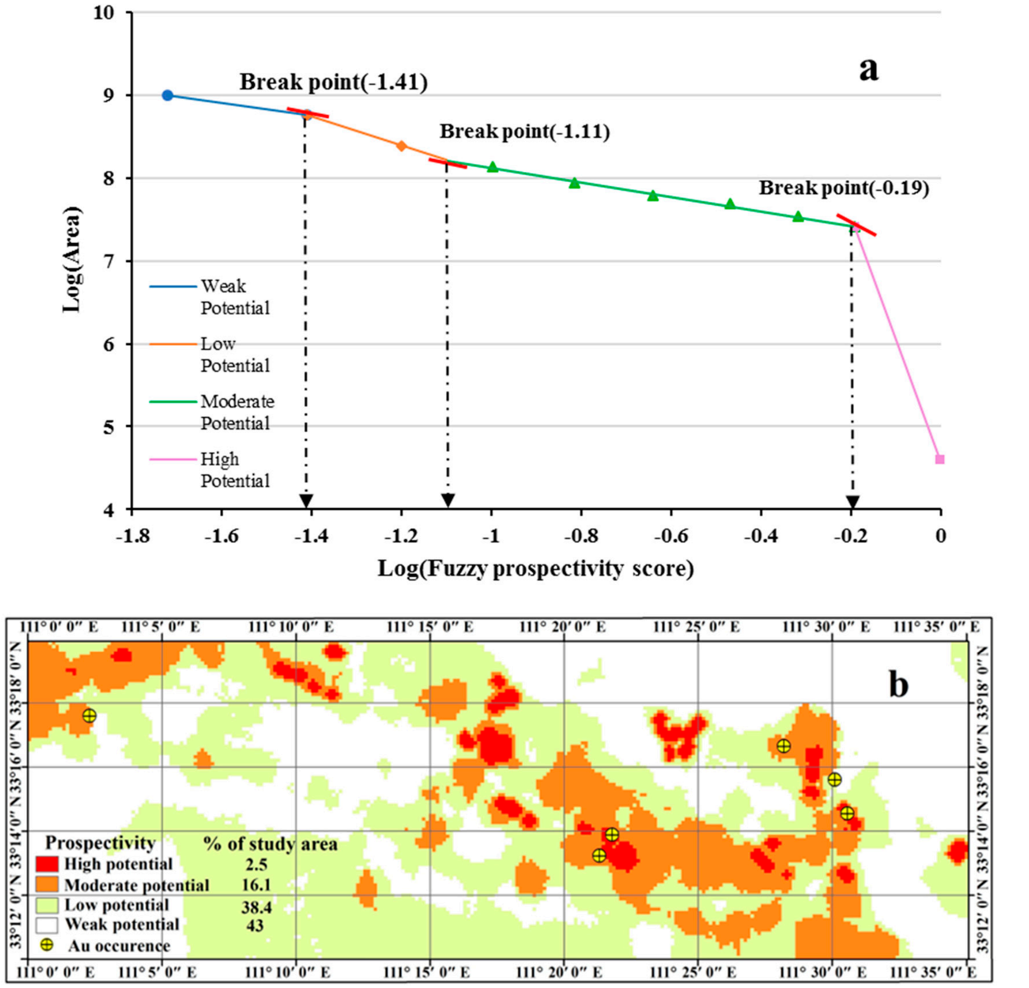

Figure 9. (**a**) Concentration–Area (C–A) model, and (**b**) prospectivity map generated by Figure 6b.

Although there was a known Au occurrence located in the low potential area, we noticed that it was very close to the moderate potential area. This may be attributed to the substitution of point position for area projection. This Au occurrence was, actually, an alteration zone about 0.76 km in length with a trend near east–west, with only its center projected on the horizontal. Therefore, it can be seen from the prospectivity map that the gold occurrence is situated less than two cells away from the favorable metallogenic area (400). In reality, the gold occurrence was partially contained by the moderate-potential areas.

6. Discussion

Previous studies have shown that Mesozoic magmatic activity in the study area may be an important source of heat and provenance for mineralization, despite its limited distribution and small outcrop area. The relatively weak activities are mainly shallow–ultra-shallow acid rocks, which are distributed along faults. Compared with common acid rocks, Au, Ag, As, Sb, Bi, Cu, and Mo are enriched in the rock mass, and their enrichment coefficients are all greater than 3.0, which may be an important source of Au in the deposit. In addition, Au was not only contained in magmatic hydrothermal fluid itself, but also probably extracted from the sedimentary strata of the wall rock, and then transported in the fracture and ductile shear zone.

The main faults in the study area are distributed in the northwest-trending direction, among which the Jianhuaizhai–Huangfengya fault, characterized by rock and ore controlling as well as unconformable forming, is the largest that has developed in the Cambrian, Sinian, and Proterozoic strata. The northeast-trending secondary faults and ductile shear zones are well developed in the study area, intersecting the northwest-trending structural line diagonally, which caused the strata and early faults to be disjointed. On the one hand, these faults can provide channels for hydrothermal migration; on the other hand, the intersection of the northwest and the secondary northeast faults is likely to form important ore-bearing spaces. As a result, the minerals in the area are generally produced in the northwest direction, and the mineral spots are mainly located at the intersection of the main structure and the secondary structure.

Different evidence layers cannot be directly compared and integrated when used for mineral prospectivity mapping because of their different dimensions. Data-driven-based logistic function, which can transform the evidence values of different magnitudes into fuzzy values within the range of 0–1 so as to represent the relative importance of mineralization, could be a suitable means. To obtain s and i by solving equations, an essentially data-driven approach is able to factually reflect the relative importance of evidence values and avoid the trial-and-error process that is usually involved in defining these two parameters [5]. There is an assumption in this process that the largest and smallest evidence values are assigned fuzzy scores close to 1 (0.99) and close to 0 (0.01), respectively. This assumption, consistent with knowledge and practical experience, has been accepted by a large number of geologists and applied in a variety of models.

In this study, four fuzzy layers of geology and geochemistry were evaluated by P–A plot. The results demonstrate that the heat source possessed the highest prediction rate, which is consistent with the strong control of orogenic gold deposits in geological hydrothermals. The prediction rate of faults also reached 61%, in a clear positive correlation with mineralization. At the same time, both multi-element geochemistry evidence layers exhibited prediction rates greater than 65%, which was in line with the SFA analysis. It should be noted that, because there are some secondary hidden faults in the region, they cannot be identified and extracted for MPM, resulting in relatively low prediction ability of faults.

When overlying, a fuzzy gamma operation was used with the recommended value of 0.95 [58]. The results revealed that the heat source, Au–As–Pb factor, and Cu–Zn–Mo–Cd factor had relatively high prediction rates, and were then integrated to derive a perspectivity map with a maximum prediction rate of 83%. This was higher than each of the evidence layers individually, or an integration of all of them. However, the prediction ability demonstrated in Figure 6a to 6c has a tendency of first increasing and then declining. We wonder whether there would be a specific prediction rate that elevates the final prediction ability with the evidence layer integrated over it and vice versa.

7. Conclusions

(1) Based on analysis of regional geological and geochemical characteristics, the epigenetic and ultra-epigenetic acid rock (such as the early Cretaceous granitic porphyry), the northwest-trending faults, and the accompanying secondary faults, as well as pathfinder elements (Au, As, Cu, Zn, Pb, Mo, and Cd) were identified and extracted as the main evidence layers in the search for orogenic gold.

(2) The data-driven-based logistic function demonstrated an excellent ability of converting evidence values of different scales into fuzzy scores with a range of 0–1, and the relative importance of the obtained fuzzy scores was approximately in line with the original evidence values. Meanwhile, in reducing the influence of subjective preferences, the data-driven-based logistic function yielded a better prediction effect than that of traditional knowledge-driven methods.

(3) Based on the analysis and application of geochemical big data, the data-driven logistic function and P–A evaluation were jointly applied to predict mineralization. The results showed that the heat source P–A plot had the highest predictive ability (81%), indicating the strong correlation between mineralization and the intermediate acid intrusive rock (vein), which is in line with the general characteristics of orogenic gold deposits.

(4) The mineralization prediction map generated in the study area, in which 83% of Au occurrences were situated in 17% of the area, confirmed the joint application of data-driven-based logistic function and P–A plot to be a simple, effective, and low-cost method for mineral prospectivity mapping that could provide guidance for further research in the study area.

Author Contributions: Conceptualization, H.B. and W.W.; investigation, Y.C., H.Z. and C.J.; writing—original draft preparation, H.B.; writing—review and editing, W.W; methodology, H.B. and Y.Y.; funding acquisition, W.W. and Y.Y. All authors have read and agreed to the published version of the manuscript.

Funding: This study was supported by the National Key R&D Program of China (Nos. 2021YFC2902003), National Natural Science Foundation of China (Nos. U1903207, 41972176 and 41872248), as well as A Project Funded by the Priority Academic Program Development of Jiangsu Higher Education Institutions (PAPD).

Data Availability Statement: Not applicable.

Acknowledgments: The authors would like to thank the editors and anonymous reviewers for their constructive comments.

Conflicts of Interest: The authors declare that they have no conflict of interest.

References

1. Yousefi, M.; Carranza, E.J.M. Fuzzification of continuous-value spatial evidence for mineral prospectivity mapping. *Comput. Geosci.* **2015**, *74*, 97–109. [CrossRef]
2. Knox-Robinso, C.M. Vectorial fuzzy logic: A novel technique for enhanced mineral prospectivity mapping, with reference to the orogenic gold mineralisation potential of the Kalgoorlie Terrane, Western Australian. *Aust. J. Earth Sci.* **2000**, *47*, 929–941. [CrossRef]
3. Abedi, M.; Norouzi, G.H.; Bahroudi, A. Support vector machine for multi-classification of mineral prospectivity areas. *Comput. Geosci.* **2012**, *46*, 272–283. [CrossRef]
4. Kreuzer, O.P.; Yousefi, M.; Nykänen, V. Introduction to the special issue on spatial modelling and analysis of ore-forming processes in mineral exploration targeting. *Ore Geol. Rev.* **2020**, *119*, 103391. [CrossRef]
5. Yousefi, M.; Nykänen, V. Data-driven logistic-based weighting of geochemical and geological evidence layers in mineral prospectivity mapping. *J. Geochem. Explor.* **2016**, *164*, 94–106. [CrossRef]

6. Behera, S.; Panigrahi, M.K.; Pradhan, A. Identification of geochemical anomaly and gold potential mapping in the Sonakhan Greenstone belt, Central India: An integrated concentration-area fractal and fuzzy AHP approach. *Appl. Geochem.* **2019**, *107*, 45–57. [CrossRef]
7. Yousefi, M.; Kamkar-Rouhani, A.; Carranza, E.J.M. Application of staged factor analysis and logistic function to create a fuzzy stream sediment geochemical evidence layer for mineral prospectivity mapping. *Geochem. Explor. Environ. Anal.* **2014**, *14*, 45–58. [CrossRef]
8. Carranza, E.J.M.; Hale, M. Wildcat mapping of gold potential, Baguio district, Philippines. *Trans. Inst. Min. Metall. Sect. B Appl. Earth Sci.* **2002**, *111*, 100–105. [CrossRef]
9. Carranza, E.J.M. Improved wildcat modeling of mineral prospectivity. *Resour. Geol.* **2010**, *60*, 129–149. [CrossRef]
10. Yousefi, M.; Carranza, E.J.M. Data-driven index overlay and boolean logic mineral prospectivity modeling in greenfields exploration. *Nat. Resour. Res.* **2016**, *25*, 3–18. [CrossRef]
11. Du, X.; Zhou, K.; Cui, Y.; Wang, J.; Zhang, N.; Sun, W. Analytical hierarchy process (AHP) and prediction-area (P-A) plot for mineral prospectivity mapping: A case study from the Dananhu metallogenic belt, Xinjiang, NW China. *Arab. J. Geosci.* **2016**, *9*, 298. [CrossRef]
12. Zadeh, L.A. Fuzzy sets. *IEEE Information and Control.* **1965**, *8*, 338–353. [CrossRef]
13. Moon, W.M.; Ping, A.N. Integration of geological, geophysical, and remote sensing data using fuzzy set theory. *Geoinformatics FCE CTU* **1991**, *2*, 171–176. [CrossRef]
14. Cheng, Q.; Agterberg, F.P. Fuzzy weights of evidence and its application in mineral potential mapping. *Nat. Resour. Res.* **1999**, *8*, 27–35. [CrossRef]
15. Carranza, E.J.M.; Hale, M. Geologically-constrained fuzzy mapping of gold mineralization potential, Baguio district, Philippines. *Nat. Resour. Res.* **2001**, *10*, 125–136. [CrossRef]
16. Luo, X.; Dimitrakopoulos, R. Data-driven fuzzy analysis in quantitative mineral resource assessment. *Comput. Geosci.* **2003**, *29*, 3–13. [CrossRef]
17. Nykänen, V.; Groves, D.I.; Ojala, V.J.; Eilu, P.; Gardoll, S.J. Reconnaissancescale conceptual fuzzy-logic prospectivity modeling for iron oxide copper–gold de-posits in the northern Fennoscandian Shield, Finland. *Aust. J. Earth Sci.* **2008**, *55*, 25–38. [CrossRef]
18. Lusty, P.A.J.; Scheib, C.; Gunn, A.G.; Walker, A.S.D. Reconnaissance-scale prospectivity analysis for gold mineralization in the Southern Uplands-Down-Longford Terrane, NorthernIreland. *Nat. Resour. Res.* **2012**, *21*, 359–382. [CrossRef]
19. Abedi, M.; Norouzi, G.H.; Fathianpour, N. Fuzzy outranking approach: A knowledge-driven method for mineral prospectivity mapping. *Int. J. Appl. Earth Obs. Geoinf.* **2013**, *21*, 556–567. [CrossRef]
20. Ford, A.; Miller, J.M.; Mol, A.G. A comparative analysis of weights of evidence, evidential belief functions, and fuzzy logic for mineral potential mapping using incomplete data at the scale of investigation. *Nat. Resour. Res.* **2016**, *25*, 19–33. [CrossRef]
21. Porwal, A.; Carranza, E.J.M.; Hale, M. Artificial neural networks for mineral potential mapping: A case study from Aravalli Province, Western India. *Nat. Resour. Res.* **2003**, *12*, 155–171. [CrossRef]
22. Carranza, E.J.M. Geochemical anomaly and mineral prospectivity mapping in GIS. In *Handbook of Exploration and Environmental Geochemistry*; Elsevier: Amsterdam, The Netherlands, 2008; Volume 11, p. 351.
23. Carranza, E.J.M.; Hale, M.; Faassen, C. Selection of coherent deposit-type locations and their application in data-driven mineral prospectivity mapping. *Ore Geol. Rev.* **2008**, *33*, 536–558. [CrossRef]
24. Zuo, R. Regional exploration targeting model for Gangdese porphyry copper deposits. *Resour. Geol.* **2011**, *61*, 296–303. [CrossRef]
25. Liu, Y.; Cheng, Q.; Xia, Q.; Wang, X. Mineral potential mapping for tungsten polymetallic deposits in the Nanling metallogenic belt, South China. *J. Earth Sci.* **2014**, *25*, 689–700. [CrossRef]
26. Liu, Y.; Cheng, Q.; Xia, Q.; Wang, X. The use of evidential belief functions for mineral potential mapping in the Nanling belt, South China. *Front. Earth Sci.* **2015**, *9*, 342–354. [CrossRef]
27. Yousefi, M.; Kreuzer, O.P.; Nykänen, V.; Hronsky, J.M.A. Exploration information systems – A proposal for the future use of GIS in mineral exploration targeting. *Ore Geol. Rev.* **2019**, *111*, 103005. [CrossRef]
28. Billa, M.; Cassard, D.; Lips, A.L.W.; Bouchot, V.; Touliere, B.; Stein, G.; Guillou-Frottier, L. Predicting gold-rich epithermal and porphyry systems in the central Andes with a continental-scale metallogenic GIS. *Ore Geol. Rev.* **2004**, *25*, 39–67. [CrossRef]
29. Chung, C.F.; Fabbri, A.G. The representation of geoscience information for data integration. *Nonrenewable Resour.* **1993**, *2*, 122–139. [CrossRef]
30. Porwal, A.; Carranza, E.J.M.; Hale, M. A hybrid neuro-fuzzy model for mineral potential mapping. *Math. Geol.* **2004**, *36*, 803–826. [CrossRef]
31. Porwal, A.; Carranza, E.J.M.; Hale, M. A hybrid fuzzy weights-of-evidence model for mineral potential mapping. *Nat. Resour. Res.* **2006**, *15*, 1–14. [CrossRef]
32. Roy, R.; Cassard, D.; Cobbold, P.R.; Rossello, E.A.; Bailly, M.; Lips, A.L.W. Predictive mapping for copper–gold magmatic-hydrothermal systems in NW Argentina: Use of a regional-scale GIS, application of an expert-guided data-driven approach, and comparison with results from a continental-scale GIS. *Ore Geol. Rev.* **2006**, *29*, 260–286. [CrossRef]
33. Carranza, E.J.M.; Ruitenbeek, F.J.A.V.; Hecker, C.; Meijde, M.V.; Meer, F.D.V. Knowledge-guided data-driven evidential belief modeling of mineral prospectivity in Cabo de Gata, SE Spain. *Int. J. Appl. Earth Obs. Geoinf.* **2008**, *10*, 374–387. [CrossRef]
34. Cassard, D.; Billa, M.; Lambert, A.; Picot, J.C.; Husson, Y.; Lasserre, J.L.; Delor, C. Gold predictivity mapping in French Guiana using an expert-guided data-driven approach based on a regional-scale GIS. *Ore Geol. Rev.* **2008**, *34*, 471–500. [CrossRef]

35. Luo, J. Statistical mineral prediction without defining a training area. *Math. Geol.* **1990**, *22*, 253–260. [CrossRef]
36. Yousefi, M.; Kamkar-Rouhani, A.; Carranza, E.J.M. Geochemical mineralization probability index (GMPI): A new approach to generate enhanced stream sediment geochemical evidential map for increasing probability of success in mineral potential mapping. *J. Geochem. Explor.* **2012**, *115*, 24–35. [CrossRef]
37. Yousefi, M.; Carranza, E.J.M.; Kamkar-Rouhani, A. Weighted drainage catchment basin mapping of stream sediment geochemical anomalies for mineral potential mapping. *J. Geochem. Explor.* **2013**, *128*, 88–96. [CrossRef]
38. Liu, Y.; Zhu, L.; Zhou, Y. Application of Convolutional Neural Network in prospecting prediction of ore deposits: Taking the Zhaojikou Pb-Zn ore deposit in Anhui Province as a case. *Acta Petrol. Sin.* **2018**, *34*, 3217–3224.
39. Zuo, R.; Xu, Y. Graph Deep Learning Model for Mapping Mineral Prospectivity. *Math. Geosci.* **2022**. [CrossRef]
40. Zhou, Y.; Chen, S.; Zhang, Q.; Xiao, F.; Wang, S.; Liu, Y.; Jiao, S. Advances and prospects of big data and mathematical geoscience. *Acta Petrol. Sin.* **2018**, *34*, 255–263.
41. Meng, Q.; Zhang, G. Geologic framework and tectonic evolution of the Qinling orogeny, Central China. *Tectonophysics* **2000**, *323*, 183–196. [CrossRef]
42. Bureau of Geology and Mineral Resources of Henan Province. *Regional Geology Records of Henan Province*; Geological Press: Beijing, China, 1989. (In Chinese with English abstract)
43. Kerrich, R.; Goldfarb, R.; Groves Garwin, S.; Jia, Y. The characteristics, origins, and geodynamic settings of supergiant gold metallogenic provinces. *Sci. China Ser. D Earth Sci.* **2000**, *43*, 1–68. [CrossRef]
44. Kerrich, R.; Wyman, D. Geodynamic setting of mesothermal gold deposits: An association with accretionary tectonic regimes. *Geology* **1990**, *18*, 882–885. [CrossRef]
45. Groves, D.I.; Goldfarb, R.J.; Gebre-Mariam, M.; Hagemann, S.G.; Robert, F. Orogenic gold deposits: A proposed classification in the context of their crustal distribution and relationship to other gold deposit types. *Ore Geol. Revs* **1998**, *13*, 7–27. [CrossRef]
46. Groves, D.I.; Goldfarb, R.J.; Knox-Robinson, C.M.; Ojala, J.; Gardoll, S.; Yun, G.Y.; Holyland, P. Late-kinematic timing of orogenic gold deposits and significance for computer-based exploration techniques with emphasis on the Yilgarn Block, Western Australia. *Ore Geol. Rev.* **2000**, *17*, 1–38. [CrossRef]
47. Craw, D.; Begbie, M.; MacKenzie, D. Structural controls on Tertiary orogenic gold mineralization during initiation of a mountain belt, New Zealand. *Miner. Depos.* **2006**, *41*, 645–659. [CrossRef]
48. Mao, J.; Goldfarb, R.J.; Zhang, Z.; Xu, W.; Qiu, Y.; Deng, J. Gold deposits in the Xiaoqinling–Xiong'ershan region, Qinling Mountains, central China. *Miner. Depos.* **2002**, *37*, 306–325. [CrossRef]
49. Chen, Y.; Pirajno, F.; Qi, J. The Shanggong gold deposit, Eastern Qinling Orogen, China: Isotope geochemistry and implications for ore genesis. *J. Asian Earth Sci.* **2008**, *33*, 252–266. [CrossRef]
50. Bai, H.; Cao, Y.; Zhang, H.; Zhang, C.; Hou, S.; Wang, W. Combining fuzzy analytic hierarchy process with concentration–area fractal for mineral prospectivity mapping: A case study involving Qinling orogenic belt in central China. *Appl. Geochem.* **2021**, *126*, 104894. [CrossRef]
51. *DZ/T 0011-2015*; Specification of Geochemical Reconnaissance Survey(1:50,000). China Geological Survey Nanjing Geological Survey Center: Nanjing, China, 2015. (In Chinese)
52. *DZ01304-2006*; The Specification of Testing Quality Management for Geological Laboratories. Ministry of Land and Resources: Beijing, China, 2006. (In Chinese)
53. Hengl, T. Finding the right pixel size. *Comput. Geosci.* **2006**, *32*, 1283–1298. [CrossRef]
54. Bishop, C.M. *Pattern Recognition and Machine Learning*; Springer Science Business Media, LLC: New York, NY, USA, 2006.
55. Pirajno, F. Intracontinental strike-slip faults, associated magmatism, mineral systems and mantle dynamics: Examples from NW China and Altay-Sayan (Siberia). *J. Geodyn.* **2010**, *50*, 325–346. [CrossRef]
56. Yousefi, M.; Carranza, E.J.M. Prediction–area (P–A) plot and C–A fractal analysis to classify and evaluate evidential maps for mineral prospectivity modeling. *Comput. Geosci.* **2015**, *79*, 69–81. [CrossRef]
57. Herbert, S.; Woldai, T.; Carranza, E.J.M.; Ruitenbeek, F.J.A.V. Predictive mapping of prospectivity for orogenic gold in Uganda. *J. Afr. Earth Sci.* **2014**, *99*, 666–693. [CrossRef]
58. Carranza, E.J.M.; Laborte, A.G. Random forest predictive modeling of mineral prospectivity with small number of prospects and data with missing values in Abra (Philippines). *Comput. Geosci.* **2015**, *74*, 60–70. [CrossRef]
59. Meng, Q.; Liu, Z.; Borders, B.E. Assessment of regression kriging for spatial interpolation – Comparisons of seven GIS interpolation methods. *Cartogr. Geogr. Inf. Sci.* **2013**, *40*, 28–39. [CrossRef]
60. Bishop, T.F.A.; Lark, R.M. The geostatistical analysis of experiments at the landscape-scale. *Geoderma* **2006**, *133*, 87–106. [CrossRef]
61. Bonham-carter, G.F. Geographic Information Systems for Geoscientists: Modelling with GIS. Computer Methods. In *The Geosciences*, 13th ed.; Pergamon Press: New York, NY, USA, 1995.
62. Mandelbrot, B.B. *Statistics of Natural Resources and the Law of Pareto*; I.B.M. Research Note NC-146; Watson Research Center: New York, NY, USA, 1962; p. 131.
63. Mandelbrot, B.B. *The Fractal Geometry of Nature*; W.H. Freeman and Company: New York, NY, USA, 1983; p. 468.
64. Mandelbrot, B.B. Self-affine fractals and fractal dimension. *Phys. Scr.* **1985**, *32*, 257–260. [CrossRef]
65. Carlson, C.A. Spatial distribution of ore deposits. *Geology* **1991**, *19*, 111–114. [CrossRef]
66. Cheng, Q.; Agterberg, F.P.; Ballantyneb, S.B. The separation of geochemical anomalies from background by fractal methods. *J. Geochem. Explor. C* **1994**, *51*, 109–130. [CrossRef]

67. Cheng, Q.; Agterberg, F.P.; Bonham-Carter, G.F. Fractal pattern integration for mineral potential estimation. *Nonrenewable Resour.* **1996**, *5*, 117–130. [CrossRef]
68. Xiang, Z.; Gu, X.; Wang, E.; Wang, X.; Zhang, Y.; Wang, Y. Delineation of deep prospecting targets by combining factor and fractal analysis in the Kekeshala skarn Cu deposit, NW China. *J. Geochem. Explor.* **2019**, *198*, 71–81. [CrossRef]
69. Hodkiewicz, P.F.; Weinberg, R.F.; Gardoll, S.J.; Groves, D.I. Complexity gradients in the Yilgarn Craton: Fundamental controls on crustal-scale fluid flow and formation of world-class orogenic-gold deposits. *Aust. J. Earth Sci.* **2005**, *52*, 831–841. [CrossRef]
70. Ford, A.; Blenkinsop, T.G. Combining fractal analysis of mineral deposit clustering with weights of evidence to evaluate patterns of mineralization: Application to copper deposits of the Mount Isa Inlier, NW Queensland, Australia. *Ore Geol. Rev.* **2008**, *33*, 435–450. [CrossRef]
71. Ghasemzadeh, S.; Maghsoudi, A.; Yousefi, M.; Mihalasky, M.J. Stream sediment geochemical data analysis for district-scale mineral exploration targeting: Measuring the performance of the spatial U-statistic and C-A fractal modeling. *Ore Geol. Rev.* **2019**, *113*, 103–115. [CrossRef]
72. Chen, D.; Wei, J.; Wang, W.; Shi, W.; Li, H.; Zhan, X. Comparison of Methods for Determining the Thresholds of Geochemical Anomalies and the Prospecting Direction-A Case of Gold Deposits in the Gouli Exploration Area, Qinghai Province. *Mineral* **2019**, *9*, 368. [CrossRef]